Seasonal Variations of Yellow Sea Fog: Observations and Mechanisms*

SU-PING ZHANG

Physical Oceanography Laboratory, and Ocean–Atmosphere Interaction and Climate Laboratory, Ocean University of China, Qingdao, China

SHANG-PING XIE

International Pacific Research Center and Department of Meteorology, SOEST, University of Hawaii at Manoa, Honolulu, Hawaii, and Physical Oceanography Laboratory, and Ocean–Atmosphere Interaction and Climate Laboratory, Ocean University of China, Qingdao, China

QIN-YU LIU

Physical Oceanography Laboratory, and Ocean–Atmosphere Interaction and Climate Laboratory, Ocean University of China, Qingdao, China

YU-QIANG YANG AND XIN-GONG WANG

Qingdao Meteorological Bureau, Qingdao, China

ZHAO-PENG REN

Physical Oceanography Laboratory, and Ocean–Atmosphere Interaction and Climate Laboratory, Ocean University of China, Qingdao, China

(Manuscript received 27 August 2008, in final form 26 April 2009)

ABSTRACT

Sea fog is frequently observed over the Yellow Sea, with an average of 50 fog days on the Chinese coast during April–July. The Yellow Sea fog season is characterized by an abrupt onset in April in the southern coast of Shandong Peninsula and an abrupt, basin-wide termination in August. This study investigates the mechanisms for such steplike evolution that is inexplicable from the gradual change in solar radiation. From March to April over the northwestern Yellow Sea, a temperature inversion forms in a layer 100–350 m above the sea surface, and the prevailing surface winds switch from northwesterly to southerly, both changes that are favorable for advection fog. The land–sea contrast is the key to these changes. In April, the land warms up much faster than the ocean. The prevailing west-southwesterlies at 925 hPa advect warm continental air to form an inversion over the western Yellow Sea. The land–sea differential warming also leads to the formation of a shallow anticyclone over the cool Yellow and northern East China Seas in April. The southerlies on the west flank of this anticyclone advect warm and humid air from the south, causing the abrupt fog onset on the Chinese coast. The lack of such warm/moist advection on the east flank of the anticyclone leads to a gradual increase in fog occurrence on the Korean coast. The retreat of Yellow Sea fog is associated with a shift in the prevailing winds from southerly to easterly from July to August. The August wind shift over the Yellow Sea is part of a large-scale change in the East Asian–western Pacific monsoons, characterized by enhanced convection over the subtropical northwest Pacific and the resultant teleconnection into the midlatitudes, the

* International Pacific Research Center Publication Number 611 and School of Ocean and Earth Science and Technology Publication Number 7752.

Corresponding author address: Suping Zhang, College of Physical and Environmental Oceanography, Ocean University of China, Qingdao 266100, China.
E-mail: zsping@ouc.edu.cn

DOI: 10.1175/2009JCLI2806.1

latter known as the western Pacific–Japan pattern. Back trajectories for foggy and fog-free air masses support the results from the climatological analysis.

1. Introduction

Sea fog often causes shipwrecks and disrupts transportation and other socioeconomic activities over the ocean and in coastal regions. The Yellow Sea experiences heavy fog over a significant fraction of the year. Figure 1 shows the number of fog days as a function of calendar month based on 30 yr of station observations. Stations on the northwest (NW) Yellow Sea coast typically record more than 50 foggy days a year while the maximum of over 80 days is found at Chengshantou (CST) station in the northern Yellow Sea.

Sea fog in the Yellow and East China Seas belongs generally to the type of fog known as advection fog, which forms as warm/moist air passes over colder water (Wang 1983). The fog season is typically from April to July along the southern coast of Shandong Peninsula (SDP) when the sea surface temperature (SST) is lower than the surface air temperature (SAT) (Figs. 1 and 2a). During the fog season, 65%~87% of the fog observations report visibility of less than 200 m at Qianliyan (QL) and Xiaomaidao (XM), with the average duration of sea fog events lasting about 2 days (Diao 1992). Longer-duration fog events are generally found from June to July, with the longest at 10 days for a 23-yr period from 1977 to 1989 (Diao 1992). The prevailing surface winds are south-southeasterlies at speeds from 2 to 10 m s^{-1} near the southern coast of SDP, advecting warm/moist air from the south (Wang 1983; Diao 1992; Zhang et al. 2005). The fact that fog days are several times more frequent on the southern (upwind) than northern (downwind) coast of SDP, such as at CD, YT, and PL (Fig. 1), corroborates the importance of warm/moist advection for Yellow Sea fog formation.

Mechanisms involved in the seasonal variations of the frequency of sea fog occurrences have been studied elsewhere. The steady northwesterly flow off the California coast, along with the upwelling and cold SSTs in response to the winds, are responsible for fog formation in the warm season (May–October) when the greatest frequency of sea fog occurs (Byers 1930; Sverdrup and Fleming 1941; Sverdrup et al. 1942; Leipper 1948). Sea fog formation via stratus lowering is found in the cool season (November–April) when SST is warmer than the surface air off the California coast (Koračin et al. 2001; Lewis et al. 2003, 2004). Tidal

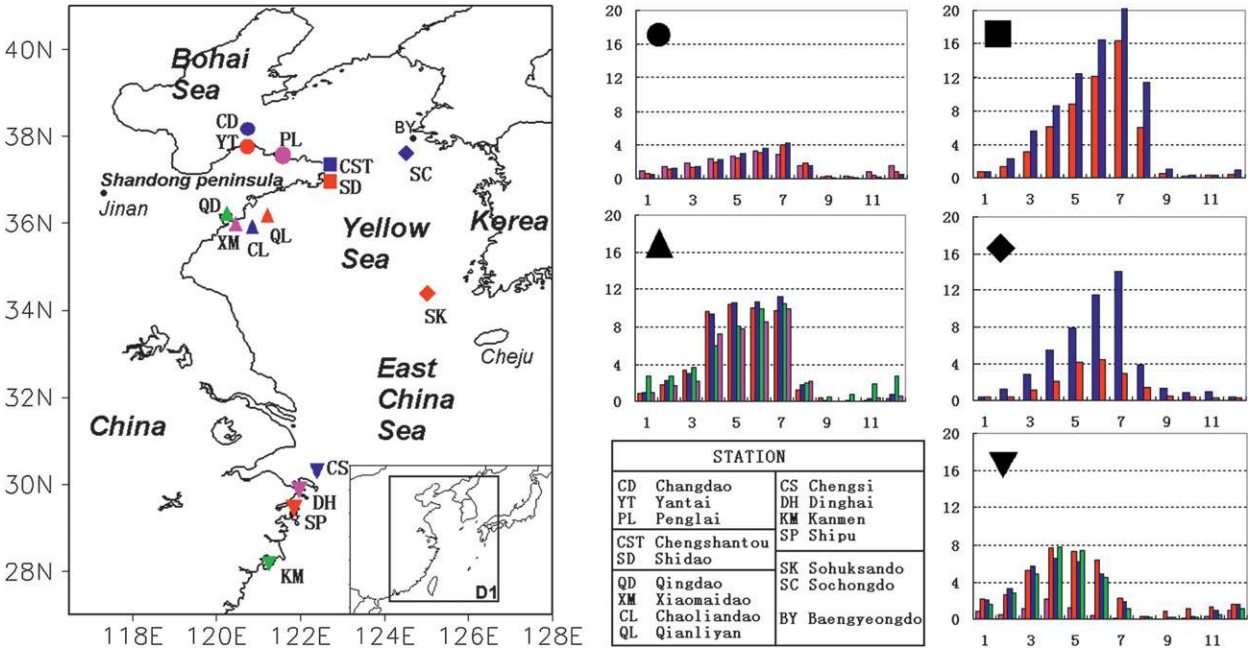

FIG. 1. Climatological seasonal cycle of the frequency (day) of fog occurrence at stations adjacent to Chinese seas. Different symbols stand for different regions: Bohai Sea (circle), northern Yellow Sea (square), northwest Yellow Sea (upward-pointing triangle), East China Sea (downward-pointing triangle), eastern Yellow Sea (diamond). Colors distinguish stations in each group. D1 is the model domain.

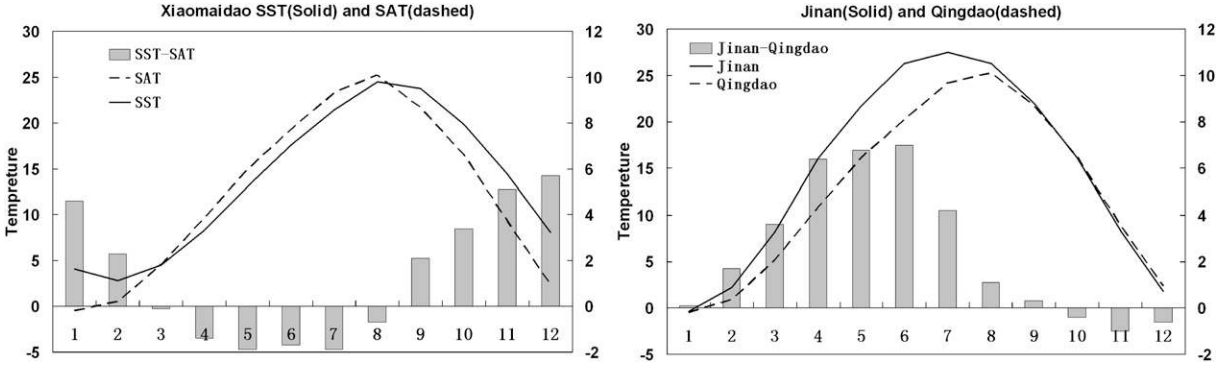

FIG. 2. (a) SST and SAT climatology for 1960–89 on the island of Xiaomaidao (36°3.2′N, 120°25.5′E) in the NW Yellow Sea near Qingdao station. (b) SAT at inland Jinan and coastal Qingdao stations, located at roughly the same latitude (See Fig. 1). The bar graphs are the (a) SST–SAT and (b) Jinan–Qingdao SAT differences labeled along the right-hand border of this figure.

mixing cools shelf regions (Su and Su 1996; Ma et al. 2004), contributing to a high frequency of sea fog occurrence and a prolonged fog season along the Korean coast of the Yellow Sea (Cho et al. 2000) and near CST at the east tip of SDP (Wang 1983) (Fig. 1) during the summer. Physical processes important for sea fog formation include the turbulent transfer of heat and moisture, the cooling of air masses that travel over colder waters near Newfoundland (Taylor 1915, 1917) and along the east coast of Scotland as well as in the neighboring North Sea (Lamb 1943), and radiative cooling at the top of the fog or stratus layer (Lamb 1943; Filonczuk et al. 1995; Koračin et al. 2001; Lewis et al. 2003, 2004).

The seasonal cycle of fog occurrence along the south coast of SDP displays two interesting features: an abrupt onset in April and an abrupt termination in August (Fig. 1). The air–sea interface is stable (SST − SAT < 0) during the April–July fog season (Fig. 2a), consistent with previous studies on necessary conditions for sea fog formation (Wang 1983). The April onset displays regional differences; the onset is abrupt along the SDP's south coast (QD, XM, CL, and QL) but is gradual along the Korean coast (Fig. 1), which is consistent with Cho et al. (2000). The regional difference suggests that the April onset is probably not due to the large-scale Asian summer monsoon, which first occurs in May in the South China Sea (Tao and Chen 1987; Wang and LinHo 2002; Zhang and Wang 2008). The abrupt retreat of sea fog in August takes place over the entire Yellow Sea basin, except at CST and some stations along the Korean west coast where the fog season is prolonged by strong SST fronts maintained by tidal mixing (Wang 1983; Cho et al. 2000). Given the smooth seasonal cycle in solar radiation, the abrupt onset and retreat of the fog season in the NW Yellow Sea are puzzling, and their cause remains poorly understood.

The present study investigates the mechanisms for the onset and termination of the Yellow sea fog season using a suite of observations and atmospheric model simulations. Specifically, we wish to address the following questions: What causes the abrupt onset along the SDP south coast in April? What then makes the fog begin gradually in the east Yellow Sea as well as in other regions? What brings the Yellow Sea fog season to an abrupt end in August? Given the prevalence of advection fog in the Yellow Sea, one expects circulation changes to be important. Indeed, we show that the onset of the Yellow Sea fog season is associated with a basin-scale anticyclonic circulation resulting from local air–sea–land interactions while the August termination is part of a large-scale shift in the East Asian–western Pacific monsoons.

Following this introduction, section 2 briefly describes the data and model used in this study. Section 3 examines seasonal variations in the stability of the atmospheric boundary layer (ABL) using atmospheric soundings and reanalysis. Sections 4 and 5 investigate processes leading to the April onset and August retreat of the Yellow Sea fog season, respectively. Section 6 is a summary.

2. Data and model

Three types of data are used in this study: surface station observations, atmospheric soundings, and analyzed products on grid points. We use observations from 13 standard weather stations operated by the China Meteorological Administration (CMA) in the Yellow and East China Seas for the period from 1971 to 2000, including four island stations (CD, CL, QL, and CS) and nine coastal stations (Fig. 1). Data for two Korean weather stations, Sochongdo and Sohuksando, are taken from 1983 to 2002 (Gao et al. 2007). We calculate the climatology of sea fog occurrence for each calendar month. Fog is reported for visibilities <1 km.

Daily soundings using an L-band radar at 0715 Beijing time (BJT) in Qingdao for the full year of 2005 are used

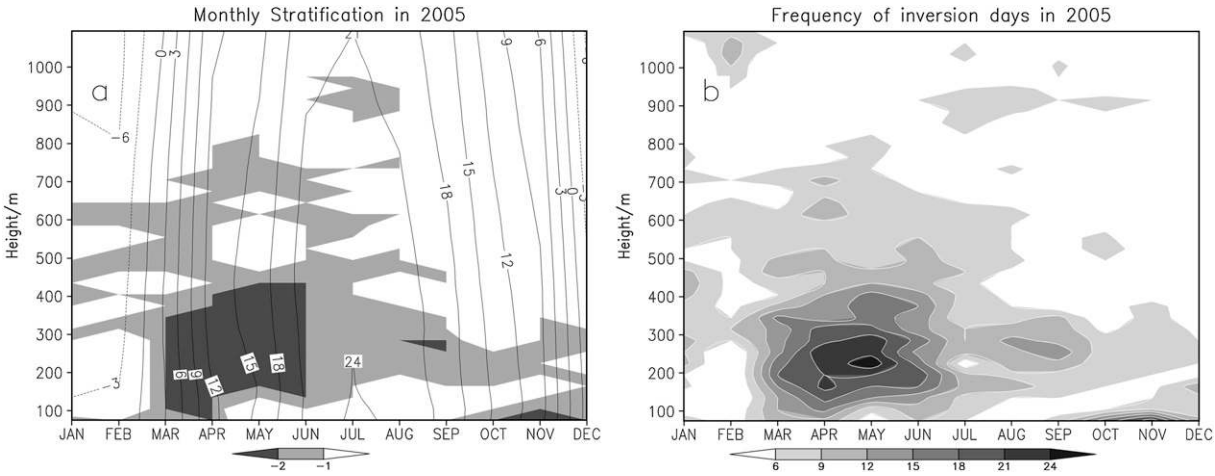

FIG. 3. (a) Monthly mean temperature (black contours, °C) in Qingdao soundings for 2005, with dark shading indicating a temperature inversion and light shading the stable layer with $dT/dz > -4$ K km^{-1} (moist-adiabatic lapse rate). (b) Days with inversion occurrence in 2005; the contour interval is 3.

to study vertical structures favorable for fog formation. The station, about 400 m inland from the coast and 75 m above sea level, is representative of atmospheric conditions over the NW Yellow Sea. Atmospheric pressure, temperature, humidity, and wind velocity are reported at a vertical resolution of 30 m. Daily soundings at Cheju and Baengnyeongdo, Korea, at 0800 BJT for 2005 were obtained online (http://weather.uwyo.edu/). The data for 1 yr (2005) contain interannual variations, which are generally smaller than the seasonal cycle, though.

The gridded datasets include the Japanese 25-yr Reanalysis (JRA-25; Onogi et al. 2007) on a 1.25° grid, the International Comprehensive Ocean–Atmosphere Dataset (ICOADS; Slutz et al. 1985; Worley et al. 2005) on a 2° grid, sea surface wind velocity from the SeaWinds scatterometer on the Quick Scatterometer (QuikSCAT) satellite (Liu et al. 2000; Liu 2002) on a 0.25° grid, and the Climate Prediction Center (CPC) Merged Analysis of Precipitation (CMAP; Xie and Arkin 1997) on a 2.5° grid.

We use the Weather Research and Forecasting model, version 2.2 (WRF v2.2), to simulate the atmospheric circulation during the onset period of the Yellow Sea fog season. The model domain extends from 21°–44°N to 110°–134°E, as shown in the bottom-right insert of Fig. 1 (D1 in Fig. 1). The domain has a horizontal resolution of 30 km and 31 sigma levels in the vertical, 11 of which are placed below $\sigma = 0.8$ or about 2 km above the ground to resolve the ABL. The National Centers for Environmental Prediction (NCEP) Final (FNL) Global Tropospheric Analyses on a 1° grid every 6 h are used as the initial and lateral boundary conditions. FNL includes the time-varying SST used for analysis. The model integration starts on 1 April 2007 and lasts for 1 month. Besides this control run, we conduct a sensitivity experiment by raising the SST by 2°C.

Two additional short simulations are made for a fog case that lasts from 1800 UTC 1 May to 0600 UTC 4 May 2008, and for a no-fog case from 0000 UTC 7 August to 1200 UTC 10 August 2008, respectively. Two-way nested domains are used, with the outer domain corresponding roughly to D1 in Fig. 1. The horizontal grid sizes are 36 and 12 km for the outer and inner domains, respectively. Details about the simulations are presented in Zhang and Ren (2009, hereafter ZR). Trajectories are obtained by back-tracking foggy and fog-free air masses to corroborate the climatological analysis.

3. Atmospheric boundary layer stability

Stable stratification in the ABL is important for sea fog (e.g., Pelié et al. 1979; Thompson et al. 1997, 2005; Ralph et al. 1998; Fu et al. 2006; Gao et al. 2007). A stable or inversion layer prevents the moisture from escaping upward and creates favorable conditions for saturation close to the sea surface. Intensive radiative cooling at the top of the fog layer promotes turbulent mixing underneath and the development of fog (Lamb 1943; Leipper 1948, 1994). Thus, a temperature inversion close to the surface favors fog formation.

Figure 3a shows monthly averaged stratification in 2005 from the Qingdao soundings as a function of month and altitude. During October–December, there is a very thin stable layer just above the surface, which is probably due to surface radiation cooling and can sometimes lead to radiation fog. A temperature inversion appears in

March in a layer 100–350 m above sea level and its occurrence becomes more frequent in April (Fig. 3b). The seasonal inversion, which lasts for 4 months from March to June, provides favorable conditions for fog formation. The inversion is observed for more than 15 days in each month from March to June in the 100–350-m layer.

The inversion disappears in the July-mean profile but a thick stable layer remains at 150–450 m (Fig. 3a), which is favorable for thicker fog formation under the conditions of sufficient moisture supply (Zhang et al. 2008). The reason for the weakened stability is possibly due to the sea surface warming. The stratification is similar from July to August, with the stable layer thickness shrinking slightly. Thus, there is something else that acts to switch off the sea fog rapidly from July to August, a topic section 5 investigates.

We have also examined the Qingdao soundings from 2006. Compared to 2005, the near-surface inversion is weak but remains robust in April 2006, setting the favorable conditions for fog (not shown).

4. April onset

The fog season onset is abrupt along the south coast of SDP, with the number of fog days increasing rapidly from March to April. On the Korean coast to the east as well as at other stations along the Chinese coast, however, the number of fog days increases gradually from March to July. This section examines the mechanisms for this asymmetry in fog onset between different regions in the Yellow Sea.

a. Inversion formation

Figure 4 shows that in April the temperature inversion is robust over the Yellow Sea. The lapse rate is about $-6.8°C\ km^{-1}$ in Qingdao, China, and $-2.5°C\ km^{-1}$ in Baengnyeongdo (BY), Korea, in the surface layer, indicative of a temperature inversion. The lapse rate becomes positive below 600 m in Cheju where warm SSTs over the warm Kuroshio Current destroy the inversion locally (Cho et al. 2000). A temperature inversion may form by the following mechanisms: surface radiation cooling, subsidence, and warm advection. Radiation inversion forms in Qingdao during early winter (Fig. 3a) but the inversion during March–June is clearly different because of its elevated base and because surface radiative cooling is much weaker than during winter. Adiabatic warming in subsidence may produce a temperature inversion, for example, in the subtropical eastern Pacific inversions form under the sinking branch of the Hadley circulation and off the U.S. west coast under downslope winds (Leipper 1948; Lewis et al. 2003).

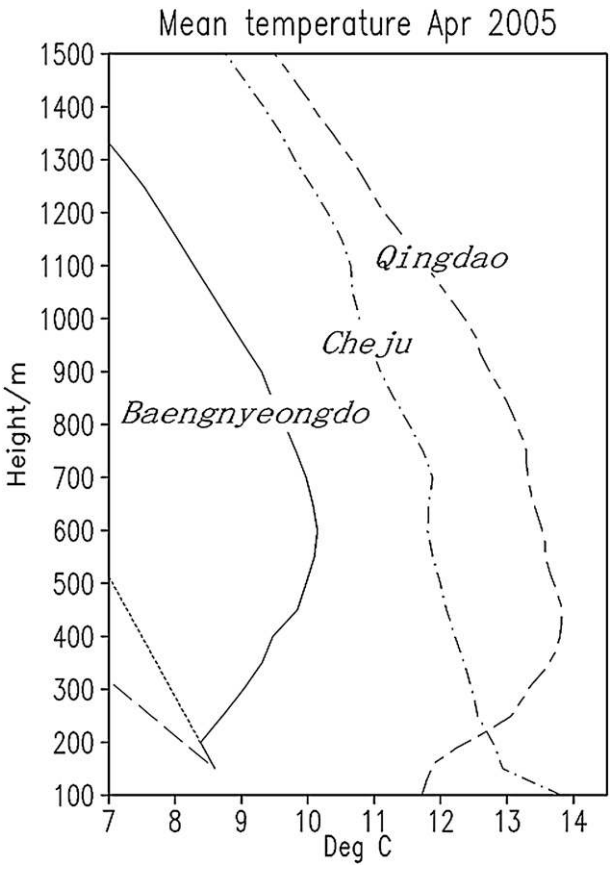

FIG. 4. Mean temperature profiles in Qingdao, Cheju, and Baengnyeongdo during April 2005. The dashed (dotted) line represents the dry- (moist-) adiabatic lapse rate.

In Qingdao during the April–July fog season, by contrast, days with low-level temperature inversions are associated with upward motion in response to warm advection from the west. Figure 5 shows vertical profiles of temperature and horizontal thermal advection in QD during April 2005. Days of major inversion formation in the 100–500-m layer are all associated with strong warm advection by west-southwesterly winds (Fig. 5a). The maximum of warm advection is at 925 hPa in the reanalysis but the exact altitude is unclear because of the coarse resolution of the dataset (Fig. 5b). We have calculated the correlation between a stratification index in the inversion layer ($T_{300m} - T_{surface}$) and the thermal advection at 925 hPa. The maximum correlation occurs with the latter leading by 1 day. The correlation is 0.73, a value exceeding the 95% significance level. The decorrelation time of the series is about 2 days. Thus, the degree of freedom for a 30-day series is 8, for which the 95% significance level is 0.632 in correlation.

In April, due to the increasing solar radiation and the differences in heat capacity between land and ocean, the

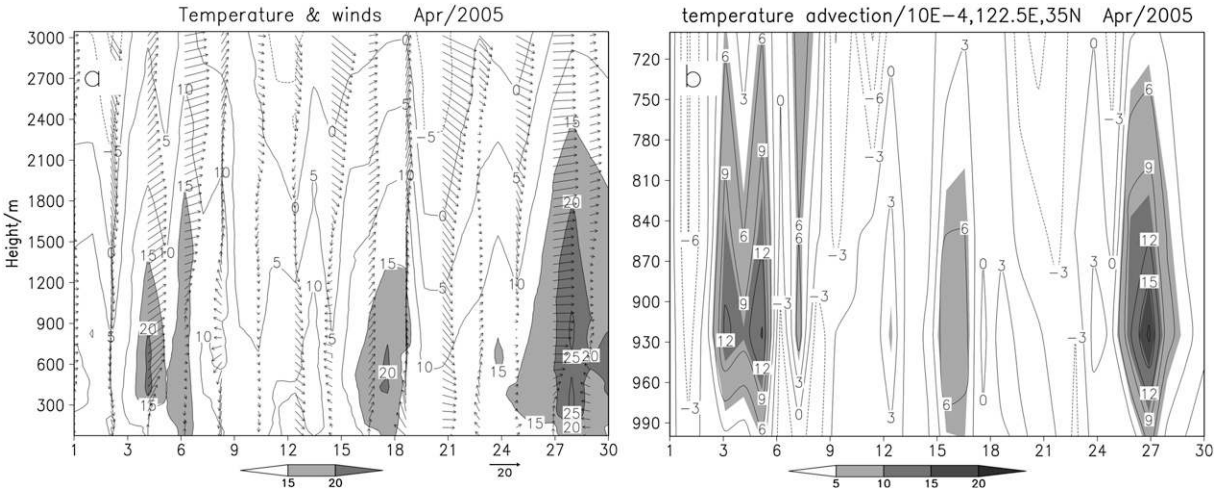

FIG. 5. Daily vertical profiles for April 2005: (a) temperature (°C) and wind velocity (m s^{-1}) from soundings in Qingdao and (b) temperature advection over the NW Yellow Sea (35°N, 122.5°E) from JRA-25 daily data. The temperature inversion and warm advection are shaded.

surface air temperature is much colder over the Yellow Sea than over continental China, with sharp gradients along the coast (Fig. 6a). For example, the SAT in inland Jinan is more than 6°C warmer than it is in coastal Qingdao (Fig. 2b). A similar eastward decrease in temperature from China to the Yellow Sea exists at 925 hPa due to turbulent mixing in the ABL (Fig. 6b). At 925 hPa, westerly offshore winds prevail in April over the Yellow Sea, advecting warm continental air in favor of inversion formation. Indeed, climatologically, the thermal advection turns positive from March to April and peaks at 925 hPa (not shown).

The April inversion results from a land–sea thermal contrast that is similar to the inversion formation mechanism along the U.S. west coast (Leipper 1948; Lewis et al. 2003) in the role of offshore warm advection. The difference over the Yellow Sea is that the offshore flow is above instead of at the surface off of California. In a zonal–vertical section, temperature advection along 36°N is greatest at 925 hPa in the western Yellow Sea (Fig. 6c). A trajectory analysis in section 4c shows that the inversion forms on the south coast of SDP when an air mass originating over land lies above that from the sea.

The zonal temperature gradient and warm advection weaken eastward as the westerlies approach the Korean Peninsula (Fig. 6c). Qingdao soundings show more frequent inversion occurrence below 400 m rather than above that level (Fig. 3) while the temperature inversions at Baengnyeongdo and Cheju lift farther upward (Fig. 4). More frequent occurrence of a temperature inversion in the lower layer of 100–350 m favors fog formation in the western to eastern Yellow Sea in April. This near-surface inversion could also be due to radiative feedback at the top of the fog layer.

b. Yellow Sea anticyclone and moisture transport

The April surface circulation features an anticyclone over the Yellow and northern East China Seas (Fig. 6a), a feature confirmed in QuikSCAT observations (not shown). This shallow anticyclone produces south-southeasterlies in the NW Yellow Sea and westerlies or northwesterlies along the Korean coast. The surface southerlies advect moist and relatively warm air (warmer than SST but cooler than the air leveling the inversion) to the NW Yellow Sea while the northwesterlies bring dry and cool air to the eastern Yellow Sea. Furthermore, the high pressure system usually increases the ABL stability, which is favorable for fog formation. As shown in Fig. 7a, a more stable air–sea interface (SST − SAT ≤ -1.5°C)[1] and higher relative humidity (>80%) are observed in the monthly mean in the NW compared to that over the eastern Yellow Sea. Specific humidity advection is positive in the NW and negative in the eastern Yellow Sea (Fig. 7b).

The anticyclone is collocated with low SATs over the ocean, suggesting the land–sea temperature contrast as its maintenance mechanism. In April, the seasonal SAT warming over the ocean lags behind that over land (Figs. 2b and 6a). Over the Yellow Sea, the cooler ABL

[1] The east–west asymmetry in stability is not very obvious in the gridded International Comprehensive Ocean–Atmosphere Data Set (ICOADS), which are subjected to heavy spatial smoothing. It is much more clear in our model simulation (Fig. 8b).

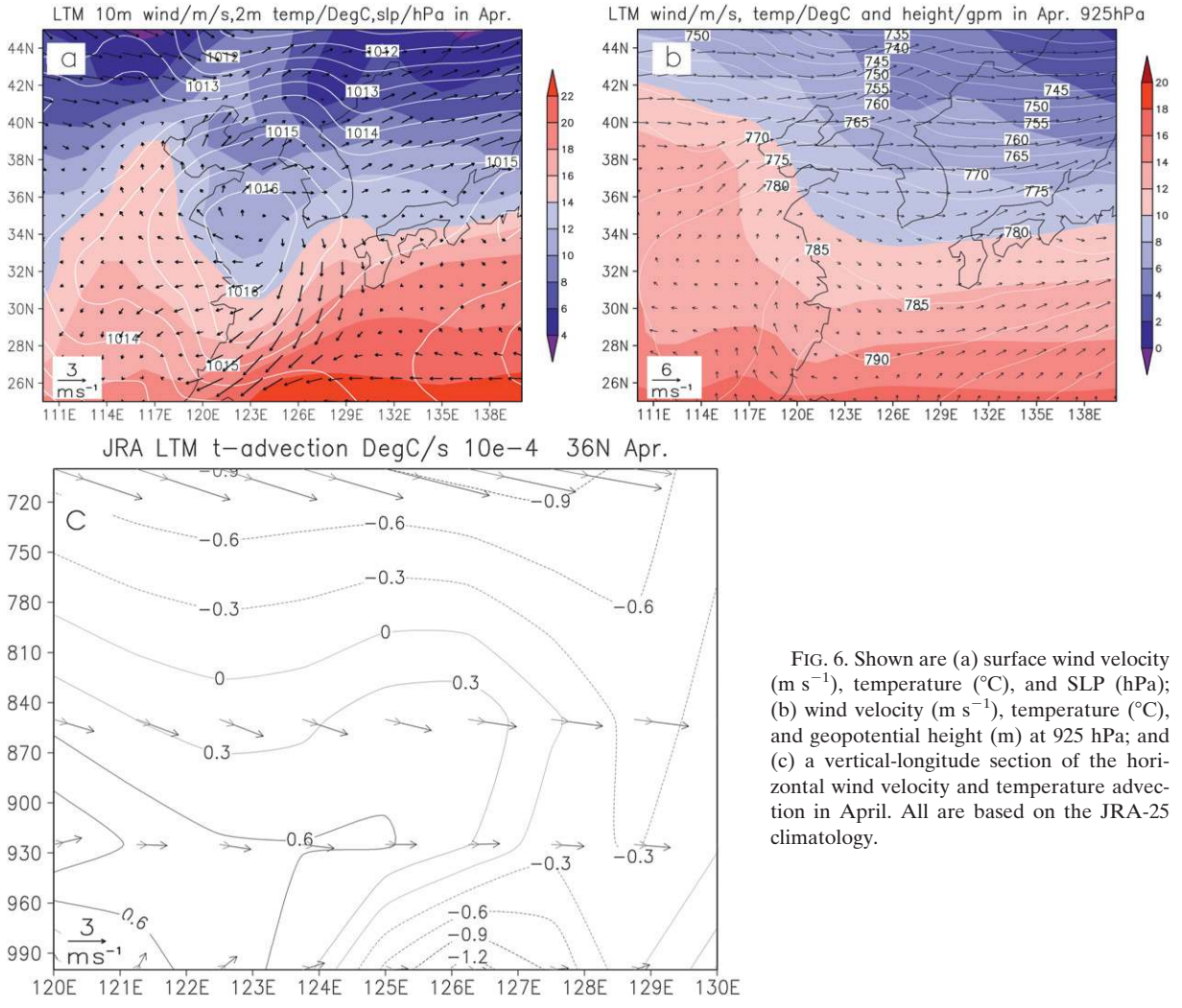

FIG. 6. Shown are (a) surface wind velocity (m s^{-1}), temperature (°C), and SLP (hPa); (b) wind velocity (m s^{-1}), temperature (°C), and geopotential height (m) at 925 hPa; and (c) a vertical-longitude section of the horizontal wind velocity and temperature advection in April. All are based on the JRA-25 climatology.

temperatures may lead to higher SLP and the surface anticyclone.

We use the regional atmospheric model WRF v2.2 to simulate this Yellow Sea shallow anticyclone. The model integration starts on 1 April 2007 and lasts for a month. The model successfully simulates the surface anticyclonic circulation (Figs. 8a–c). Its intensity is stronger in the month-long simulation than in the observed climatology by a factor of 2, possibly because of interannual variability. The surface atmospheric temperature is higher over the western Yellow Sea compared to the eastern region, as the southerlies maintain a warm advection on the western flank of the anticyclone, resulting in a stable surface stratification (SST − SAT ≤ 0°C) over an extended area of the western Yellow Sea (Fig. 8b). The model also successfully simulates the shallow temperature inversion in Qingdao but the inversion weakens in intensity eastward (Fig. 8c), consistent with sounding observations (Fig. 4).

To test the hypothesis that a land–sea temperature contrast maintains the shallow anticyclone, we conduct a sensitivity run by adding an SST increase of 2°C at ocean grid points in the model domain. Figure 9 shows the differences from the control run. The SST warming weakens the anticyclone over the ocean. Over the Yellow Sea in particular, the southerlies weaken by 1 m s^{-1} in the SST warming run, supporting the idea that a thermal high mechanism that cool SSTs over the ocean contributes to the anticyclone formation. (The weak SAT responses in the Bohai and Yellow Seas compared to that in the East China Sea are presumably because of their small sizes and hence the strong advection and mixing with continental air.)

The Yellow Sea shallow anticyclone causes asymmetry in fog occurrence between the western and eastern basins. In the western basin, the pronounced onshore southerly component advects warm and humid air from the south, in favor of fog formation with high surface

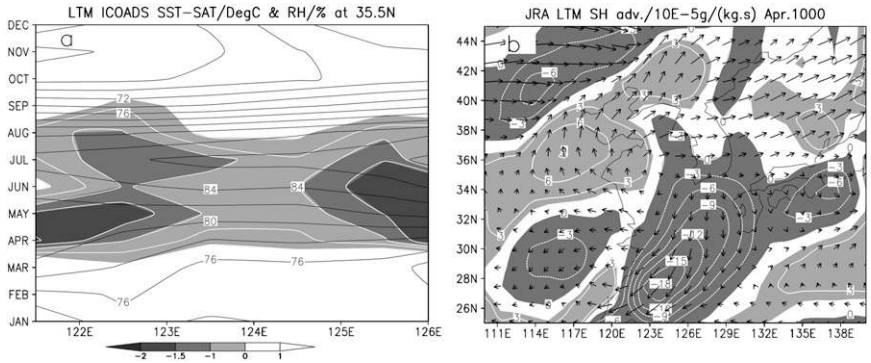

FIG. 7. (a) SST – SAT (°C; SST − SAT < 0 is shaded and contoured in white) and relative humidity (%) along 35.5°N as a function of longitude and month. Both are based on the International Comprehensive Ocean–Atmosphere Data Set (ICOADS) climatology. (b) Advection of specific humidity at 1000 hPa from the JRA-25 climatology. Dark (light) shading represents positive (negative) advection.

stability and high relative humidity (Figs. 7a and 7b). In the eastern basin, by contrast, the lack of such strong warm/moist advection leads to fewer fog days in April. As the land surfaces warms from March to April, the ocean remains cool. The resultant formation of the Yellow Sea anticyclone gives rise to the abrupt onset of the fog season on its western coast (Qingdao, China) but not on the eastern coast (Shochongdo, Korea). The northern coast of SDP has fewer fog days because the surface winds blow from land to sea.

c. *A case study*

A sea fog event on 2–3 May 2008 has been studied by ZR. At 0000 UTC 2 May, the western Yellow Sea is controlled by south-southeasterlies on the western flank of a cool surface high (Fig. 10a). Meanwhile, a low trough lies over mideastern China at 925 hPa, leading to south-southwesterly offshore flow over the NW Yellow Sea (not shown). Such a synoptic pattern is in evidence starting on 28 April. The offshore winds above 400 m advect warm air to the cool sea surface, producing a temperature inversion in Qingdao. The surface southeasterlies bring moisture from the East China Sea, with relative humidity close to 100% in the lowest 300 m (Fig. 10a, right). All of this is favorable for the fog formation observed during the evening of 2 May.

The simulation of this fog event by WRF is in good agreement with the observations (ZR). Backtracked trajectories of a slab of air starting near QD are obtained starting from the time of the fog event (Fig. 10b). The air parcel near the sea surface (10~100 m) has a sea-based

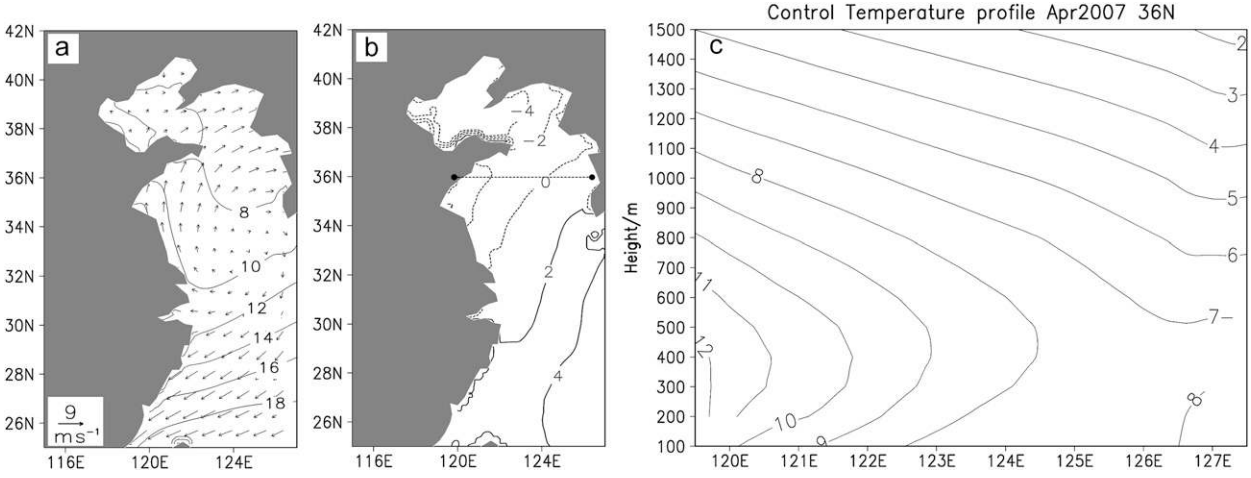

FIG. 8. Control simulation for April 2007: (a) temperature (contours, °C) and wind velocity (m s^{-1}) at 1000 hPa, (b) surface stability (SST − SAT, °C), and (c) a vertical section of temperature (°C) along 36°N as shown in (b) by a straight line.

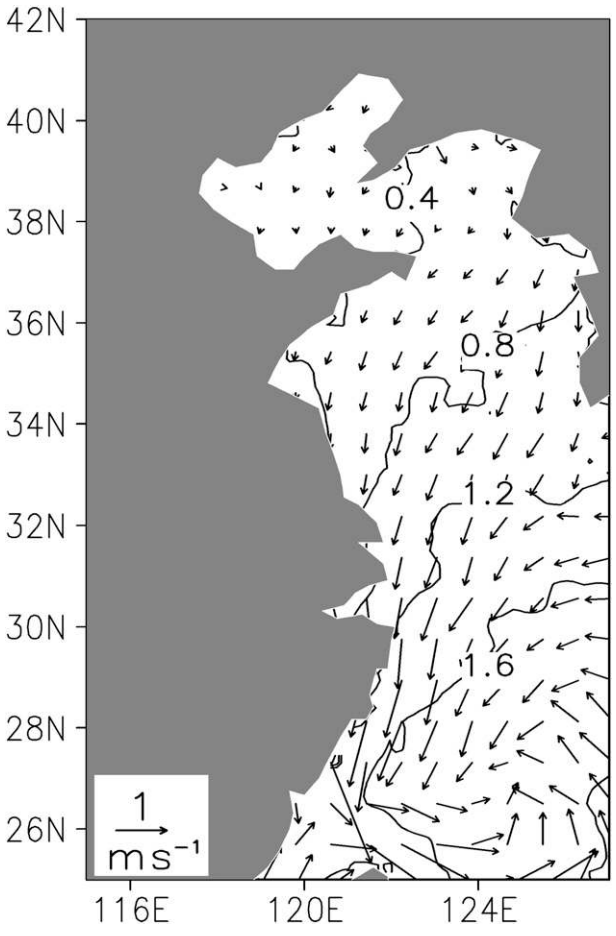

FIG. 9. The model response in April, expressed as differences from the control run, to the SST increase: temperature (contours, °C) and wind velocity (m s^{-1}).

path history from the East China Sea to the Yellow Sea. Its temperature decreases slowly at first as a result of airmass modification by cool SSTs, and then proceeds rather quickly after the fog occurs (Fig. 10b, right), indicating the effects of fog-top longwave radiation. Associated with the rapid cooling, subsidence is found at the fog top (not shown). These adjustments are very similar to those of the formation of haar or sea fog in the North Sea (Douglas 1930; Lamb 1943) and near Newfoundland (Taylor 1915, 1917), where the sea fogs result from the cooling of warm air by the cold sea and turbulent transport of heat is found between the cold sea and the adjoining warmer air. The radiative cooling at the cloud top is also the primary mechanism for the stratus lowering to form sea fog off the coast of California (Koračin et al. 2001; Lewis et al. 2003).

The air parcel at 500~1000 m has a long land-based history of traveling from southeast China northward across the NW Yellow Sea to QD (Fig. 10b, left). The temperature of the air mass increases gradually. The land-based air masses overlie the sea-based air masses near the southern coast of SDP, forming a strong temperature inversion. Meanwhile, the relative humidity of the air masses at the 10~100 m layer increases and saturation occurs approaching the NW Yellow Sea. Satellite images, as well as data from coastal stations and buoys, confirm the model results (ZR).

The results from this case analysis support the results from our climatological study, regarding the importance of the warm advection for inversion formation and role of the shallow anticyclonic circulation in causing the differences in sea fog onset between the west and east coasts of the Yellow Sea.

d. Comparison with previous studies elsewhere

The land–sea contrast is important for the April onset of the sea fog season over the Yellow Sea. Such a thermal contrast is also crucial for the formation of sea fog along the U.S. west coast. In Leipper's conceptual model, the Pacific surface anticyclone extends inland to produce northeasterly or easterly offshore flows that bring warm air from the continent to the cold sea to start sea fog (Leipper 1948). But there are some differences. In our study the low trough in central-eastern China brings the west-to-southwesterly warm offshore flow to the cool Yellow Sea to establish the inversion, and the offshore flow is at 925 hPa rather than at the surface. In addition, the shallow cool anticyclone at the surface of the Yellow Sea, which results from the land–sea contrast, is especially important in the east–west asymmetry of the fog occurrence.

Another difference compared with the sea fog off the U.S. west coast is related to the vertical motion. The large-scale subsidence strengthens the inversion and lowers the marine stratus to form sea fog off the California coast (Koračin et al. 2001; Lewis et al. 2003), but almost no large-scale subsidence is found in the process of sea fog formation over the Yellow Sea. In neither the land- or sea-based trajectories in Fig. 10b do the air masses sink significantly during their long paths (not shown), which is consistent with another fog case study from March 2005 (Gao et al. 2007). Downward motion exists in response to the radiative cooling at fog top, which is similar to sea fog formation in the North Sea (Douglas 1930; Lamb 1943) and near Newfoundland (Taylor 1915, 1917). This radiative cooling at the top of the fog layer can both promote the turbulence and mixing in the fog layer and have a positive feedback to the surface high pressure system over the Yellow Sea.

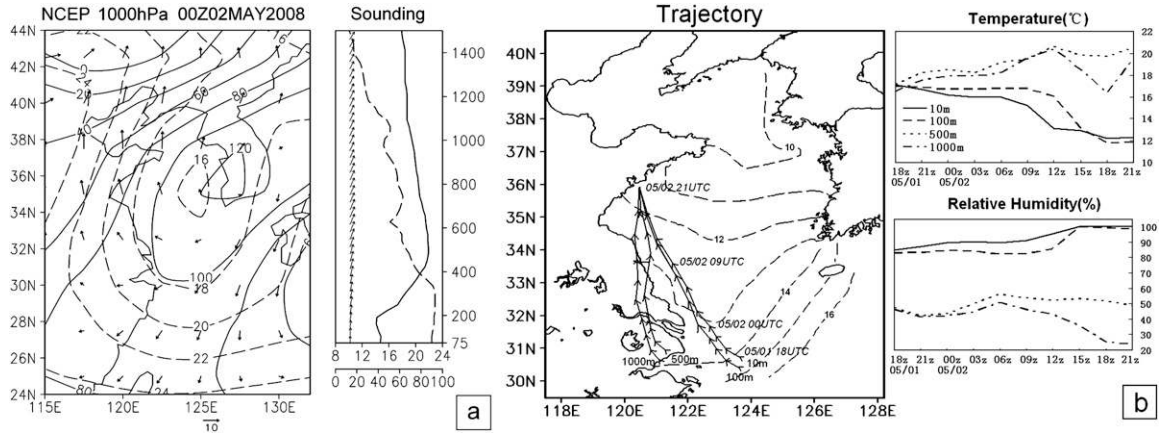

FIG. 10. (a) (left) Synoptic map at 1000 hPa and (right) sounding at QD at 0000 UTC 2 May 2008. In the synoptic map, dashed contours are for temperature (°C) and solid ones for geopotential height (m). In the sounding map, the solid line stands for temperature and the dashed line for relative humidity. (b) (left) Trajectories of air masses (lines with arrows) backtracked from QD and SST (°C) at 1800 UTC 1 May 2008 (arrows denote displacements at 3-h intervals); (right) variations of temperature and relative humidity along the trajectories. All based on WRF simulations.

5. Abrupt termination in August

The frequency of sea fog occurrence suddenly drops from its peak in July to almost none in August over the entire Yellow Sea. This abrupt termination is puzzling as the SST and land temperature change only gradually from July to August (Fig. 2). This section investigates the cause of the August termination of the Yellow Sea fog season.

a. ABL stability

From July to August, SAT in inland Jinan begins to decrease while SST continues to increase over the

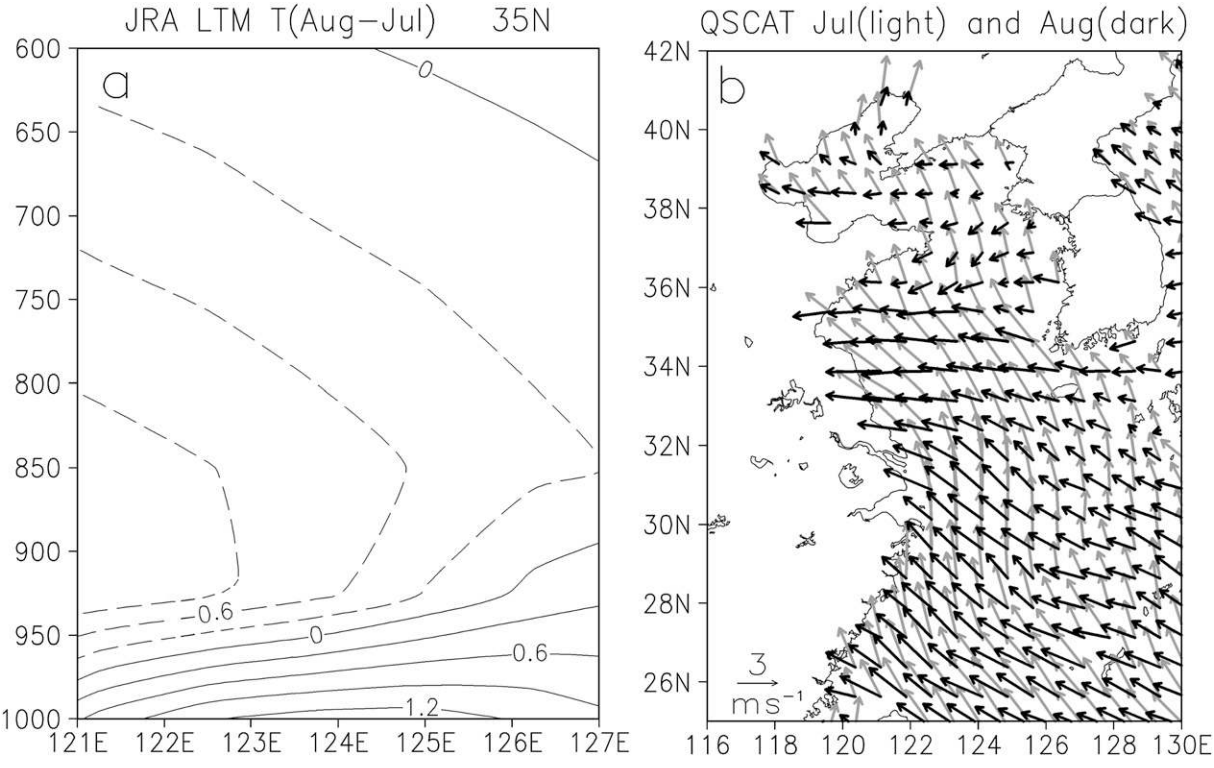

FIG. 11. (a) August–July difference in temperature (°C) along 36°N. (b) QuikSCAT wind velocity (m s^{-1}) for July (light) and August (dark). (Data in the left panel are from the JRA-25 climatology; QuikSCAT data are averaged from 2000 to 2007.)

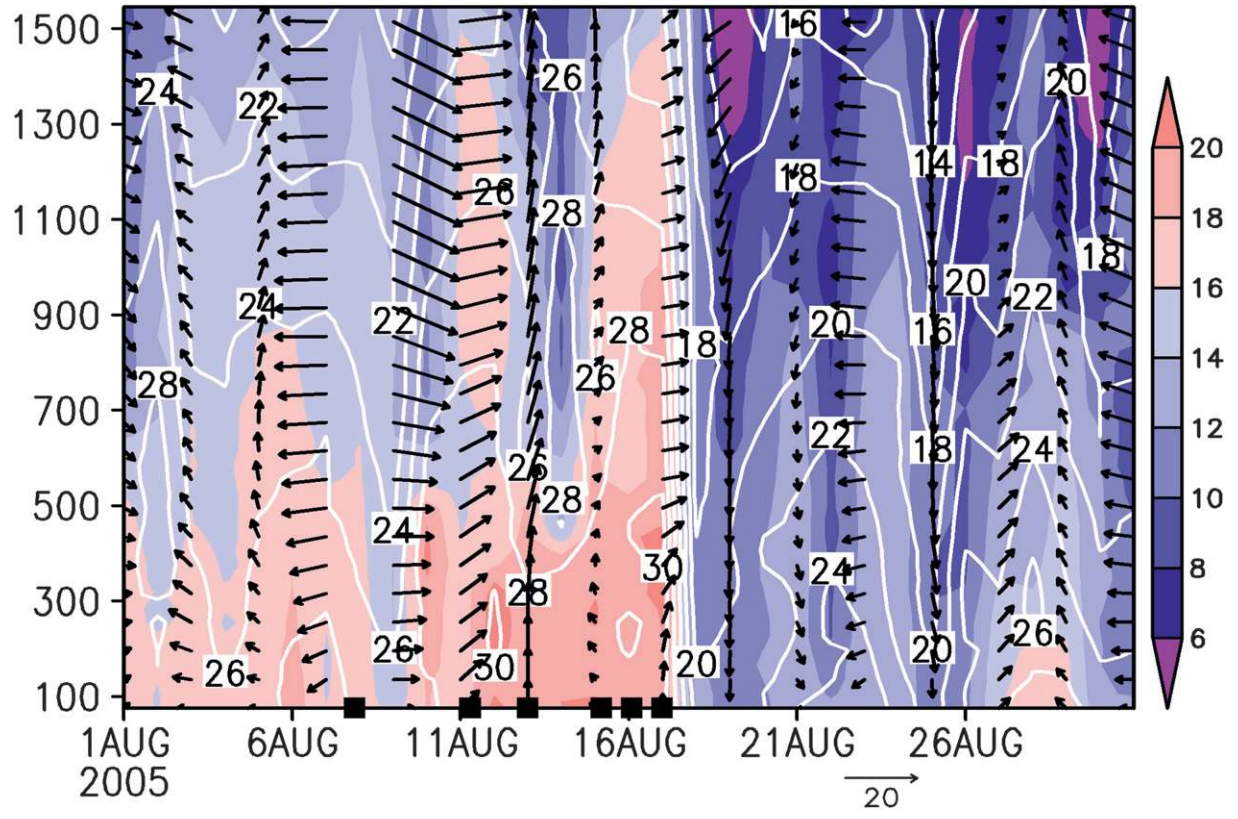

FIG. 12. Daily specific humidity (g kg^{-1}, shaded), virtual temperature (°C, contours), and horizontal wind velocity (m s^{-1}) for August 2005. Fog days are marked with the filled rectangles.

Yellow Sea (Fig. 2). The asynchronous changes in land and sea temperatures lead to a vertical dipolar pattern of temperature change in the lower troposphere, with positive changes near the surface and negative ones above (Fig. 11a). The vertical structure weakens the atmospheric stability in the ABL, which is unfavorable for fog formation.

In 2005, the stable layer in the ABL shrinks slightly from July to August but otherwise the ABL structure is similar between the 2 months (Fig. 3a). The inversion occurrence is also similar below 400 m but shows a decrease in a layer above 400–600 m (Fig. 3b). The latter change appears to be consistent with the decreased stability in the JRA climatology (Fig. 11a).

The termination of the 2005 fog season in Qingdao is an abrupt event taking place in mid-August (Fig. 12). The first half of August differs from the second half in temperature, humidity, prevailing winds, and fog days. The southerly or southeasterly winds are replaced with easterlies or northerlies winds in the second half. There are six fog days during the first half of August but no fog is observed during the second half. On 19 August 2005, the northeasterly winds bring cool and dry air to the Yellow Sea, disrupting the stable stratification, ending the sea fog season abruptly.

b. Wind shift

Prevailing winds change the direction abruptly from July to August, from southerly to easterly (Fig. 11b). This wind shift is likely an important factor in the process of terminating the fog season as it disrupts the warm and moist advection from the south. Associated with the wind shift and the warming at sea surface, the near-surface stability weakens and is close to being neutral (Fig. 7a). Relative humidity also begins to decrease rapidly as the southerly advection disappears.

The easterly wind shift over the Yellow and East China Seas is part of a series of much larger-scale changes in the atmospheric circulation spanning from East Asia to the northwest Pacific. Figure 13 shows August–July differences in the precipitation and circulation climatologically. From July to August, atmospheric convection intensifies over the subtropical northwest Pacific (Ueda et al. 1995), exciting a northward-propagating, barotropic wave train with low pressure in the subtropics and a high in the midlatitudes. This meridional dipole, called the western Pacific–Japan pattern (Nitta 1987), is a robust teleconnection pattern in summer associated with variability in the northwest

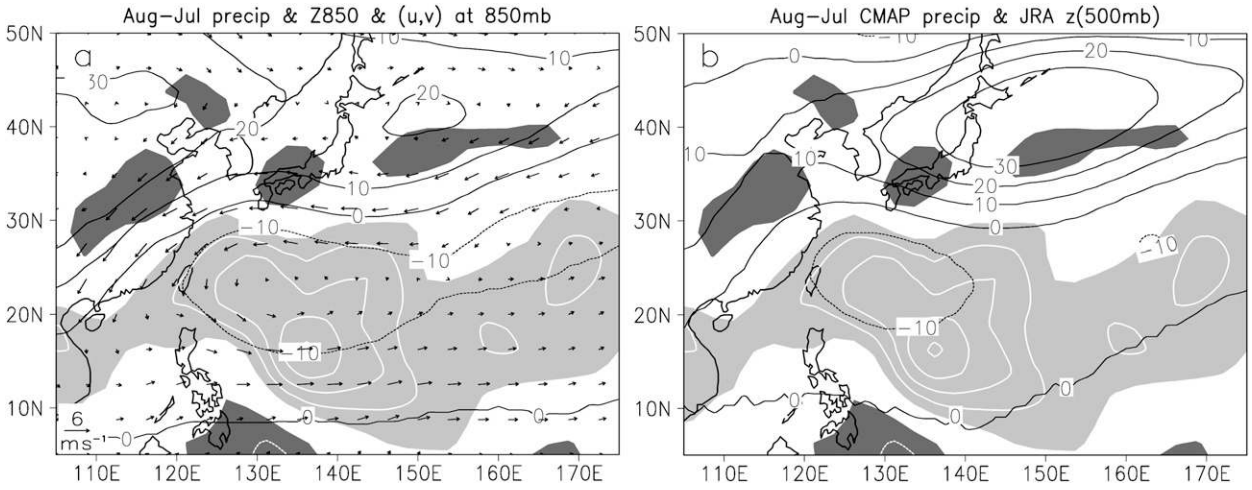

FIG. 13. August − July differences: precipitation (shaded in mm day^{-1}) and geopotential height (black contours in gpm) at (a) 850 and (b) 500 hPa. In (a), the wind velocity (m s^{-1}) at 850 hPa is superimposed. Light (dark) shading represents a positive (negative) precipitation difference, and the contour interval is 2 mm day^{-1}. Data are based on the JRA-25 and the Climate Prediction Center merged Analysis of Prediction (CMAP) climatology.

Pacific convection (e.g., Huang and Li 1988; Kosaka and Nakamura 2006). Seasonal variations of large-scale convective activity and wind over the western Pacific are connected with the Asian–northwest Pacific summer monsoon (Ueda et al. 2009). The Yellow and East China Seas are situated between the subtropical low and midlatitude high in Fig. 13 and therefore see an easterly wind shift in the seasonal march from July to August. The wind shift signals the end of the favorable conditions for sea fog, which include the moist advection from the south. Thus, the August termination of Yellow Sea fog is not a local phenomenon but is associated instead with large-scale changes in the atmosphere.

c. *Case study*

The WRF model simulation results are applied to obtain the backtracked trajectories of air masses within a Lagrangian framework for a no-fog case. On 7 August 2008, influenced by the development of an anticyclone over Japan and low pressure east of Taiwan, the Japan Sea and the Yellow Sea are controlled by easterly winds, with no fog observed (not shown). When traced back from QD, the surface air mass (10 m) maintains a nearly constant temperature across the Yellow Sea where the SST gradient is weak in the east–west direction (Fig. 14, left). Over the Korean Peninsula, the surface air mass is heated by the warm surface as part of the diurnal cycle. Similar surface warming is also found in the process of the sea fog's demise off the California coast (Lewis et al. 2003). In contrast with the surface warming, the temperature at 500 m does change remarkably along the trajectory, thereby weakening the ABL stability over the Yellow Sea (Fig. 14, top right), consistent with the vertical dipolar pattern in Fig. 11a. Along the trajectories, the relative humidity of the air masses is well below saturation (Fig. 14, bottom right). This case illustrates that easterly winds are unfavorable for fog formation over the Yellow Sea.

6. Summary

We have used a suite of in situ and satellite observations to examine the seasonal cycle of Yellow Sea fog. Yellow Sea fog is most frequently observed during April–July. Our results confirm previous studies that the southerly winds and their advection of warm and humid air are important for Yellow Sea fog during April–July, as illustrated by the contrast between Yantai and Qingdao, two cities only 200 km apart on the north and south coasts of the Shandong Peninsular, respectively. Fog rarely occurs in Yantai but is frequently observed in Qingdao. The April onset of the fog season displays pronounced spatial variations: it is abrupt off the south coast of SDP but gradual along the Korean coast. The termination of the sea fog season is abrupt along both the Chinese and Korean coasts of the Yellow Sea except some for in areas with strong tidal mixing. We have investigated mechanisms for the peculiar abrupt onset and termination of the Yellow Sea fog season. Note that the SSTs are even cooler and the cooler areas are larger along the west coast of the Korean Peninsula due to stronger tidal mixing compared with the situations near CST in summer (Cho et al. 2000; Bao et al. 2002), yet the

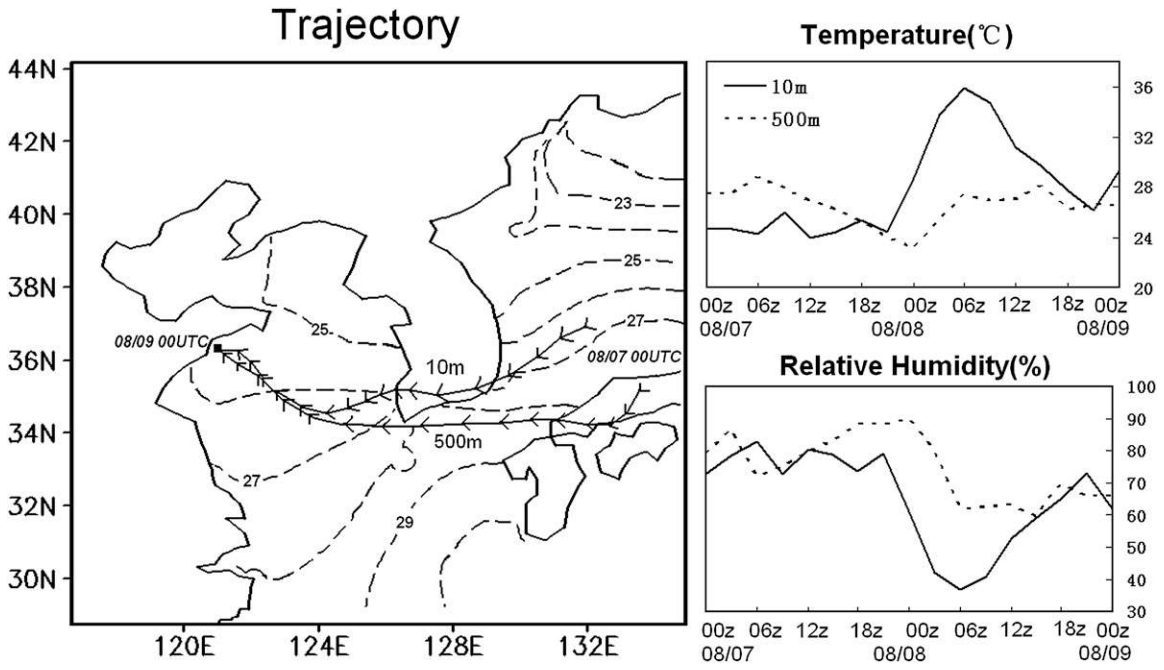

FIG. 14. As in Fig. 11 but at 0000 UTC 7 Aug 2008.

differences in SSTs do not affect the conclusions made in the present study.

From March to April, the seasonal warming over the Yellow Sea lags behind that over the surrounding land areas. At 925 hPa, the prevailing westerlies advect warm continental air over the cool Yellow Sea, forming a temperature inversion that helps trap moisture in the ABL in favor of fog formation. The land–sea differential heating also gives rise to a shallow thermal high with surface anticyclonic circulation over the Yellow and northern East China Seas. This surface anticyclone explains the east–west asymmetry in fog onset between the Chinese (abrupt) and Korean (gradual) coasts. The southerly winds on the western flank of the anticyclone sustain warm and moist advection, favoring fog formation there to the eastern basin. In addition, radiative cooling at the cloud top provides a positive feedback for the shallow high. A case study viewed within a Lagrangian framework supports the mechanisms for inversion and sea fog formation.

While the April onset is strongly influenced by the shallow anticyclone resulting from the local land–sea temperature contrast, the August withdrawal of the fog season is associated basin wide with large-scale changes in the East Asian–western Pacific monsoons. From July to August, the intensification of atmospheric convection over the subtropical NW Pacific excites a barotropic wave train. The resultant meridional dipole pattern of a geopotential decrease over the subtropics and an increase in the midlatitudes causes the prevailing winds to shift from southerly to easterly over the Yellow Sea. This wind shift terminates the southerly warm/moist advection that sustains Yellow Sea fog from April to July.

Advection fog is commonly observed elsewhere. Yellow Sea fog follows the commonly known mechanism with a warm, humid surface air mass flowing over cool water surface under a low inversion. The most important contribution of this study is perhaps the identification of circulation patterns that give rise to the onset and termination of the sea fog season over the Yellow Sea. During the core fog season of the Yellow Sea (May–July), the surface southerlies are part of the planetary-scale circulation pattern between the thermal low over China and the North Pacific subtropical high (Xie and Saiki 1999), feeding a persistent rainband called the mei-yu in China and the baiu in Japan. Blowing down the SST gradient, these monsoonal southerlies give rise to sea fog over the Yellow Sea and in the Kuroshio–Oyashio extension region east of Japan (Tokinaga et al. 2009).

On the seasonal time scale, the abrupt onset of subtropical NW Pacific convection is associated with the end of the mei-yu–baiu rainy season in China and Japan (Ueda et al. 1995, 2009). On interannual time scales, changes in subtropical NW Pacific convection are also associated with a similar meridional wave train called the western Pacific–Japan pattern (Nitta 1987; Kurihara and Tsuyuki 1987). Interannual anomalies of subtropical

NW Pacific convection tend to occur during the decay phase of an El Niño–Southern Oscillation (ENSO) event (Xie et al. 2009), raising the possibility of there being a tropical influence on Yellow Sea fog variability. The Yellow Sea fog season indeed displays interannual variations. For instance, there are 50 fog days in 2006 but only 24 fog days in 2007 in Qingdao during April–July. Interannual variations in sea fog occurrence are a topic of our future research.

Acknowledgments. We wish to thank J. Lewis and two anonymous reviewers for constructive comments. We also wish to thank Peng-Fei Gong for managing the sounding data, and Zuo-Wei Ding for her help with some of the figures. This work is supported by Grants 2006AA09Z149 from the Ministry of Science and Technology of China, 2004GG2208111 from the Department of Science and Technology of Shandong Province, NSFC 40975003, the Green Card Project of the Ocean University of China, the Changjiang Scholar Program of the Ministry of Education of China, the U.S. National Aeronautics and Space Administration, and the Japan Agency for Marine–Earth Science and Technology.

REFERENCES

Bao, X. W., X. Q. Wan, G. P. Gao, and D. X. Wu, 2002: The characteristics of the seasonal variability of the sea surface temperature field in the Bohai Sea, the Huanghai Sea and the East China Sea from AVHRR data (in Chinese). *Acta Oceanol. Sin.,* **24** (5), 125–133.

Byers, H., 1930: Summer sea fogs of the central California coast. *Publ. Geogr,* **3,** 291–338.

Cho, Y.-K., M.-O. Kim, and B.-C. Kim, 2000: Sea fog around the Korean Peninsula. *J. Appl. Meteor.,* **39,** 2473–2479.

Diao, X. X., 1992: Statistical analysis of sea fog near Qingdao adjacent sea (in Chinese). *Mar. Forecasts,* **9** (3), 45–55.

Douglas, C., 1930: Cold fogs over the sea. *Meteor. Mag.,* **65,** 133–135.

Filonczuk, M. K., D. R. Cayan, and L. G. Riddle, 1995: Variability of marine fog along the California coast. Scripps Institution of Oceanography Rep. 95-2, 91 pp.

Fu, G., J. Guo, S.-P. Xie, Y. Duan, and M. Zhang, 2006: Analysis and high-resolution modeling of a dense sea fog event over the Yellow Sea. *Atmos. Res.,* **81,** 293–303.

Gao, S. H., H. Lin, B. Shen, and G. Fu, 2007: A heavy sea fog event over the Yellow Sea in March 2005: Analysis and numerical modeling. *Adv. Atmos. Sci.,* **24,** 65–81.

Huang, R. H., and W. J. Li, 1988: Influence of the heat source anomaly over the tropical western Pacific on the subtropical high over East Asia and its physical mechanism. *Chin. J. Atmos. Sci,* **14,** 95–107.

Koračin, D., J. Lewis, W. Thompson, C. Dorman, and J. Businger, 2001: Transition of stratus into fog along the California coast: Observations and modeling. *J. Atmos. Sci.,* **58,** 1714–1731.

Kosaka, Y., and H. Nakamura, 2006: Structure and dynamics of the summertime Pacific–Japan (PJ) teleconnection pattern. *Quart. J. Roy. Meteor. Soc.,* **132,** 2009–2030.

Kurihara, K., and T. Tsuyuki, 1987: Development of the barotropic high around Japan and its association with Rossby wave-like propagations over the North Pacific: Analysis of August 1984. *J. Meteor. Soc. Japan,* **65,** 237–246.

Lamb, H., 1943: Haars or North Sea fogs on the coasts of Great Britain. Meteorology Office Publication M. M. 504, 24 pp.

Leipper, D. F., 1948: Fog development at San Diego, California. *J. Mar. Res.,* **VII,** 337–346.

——, 1994: Fog on the U.S. west coast: A review. *Bull. Amer. Meteor. Soc.,* **75,** 229–240.

Lewis, J., D. Koračin, R. Rabin, and J. Businger, 2003: Sea fog off the California coast: Viewed in the context of transient weather systems. *J. Geophys. Res.,* **108,** 4457, doi:10.1029/2002JD002833.

——, ——, and K. Redmond, 2004: Sea fog research in the United Kingdom and United States: Historical essay including outlook. *Bull. Amer. Meteor. Soc.,* **85,** 395–408.

Liu, W. T., 2002: Progress in scatterometer applications. *J. Oceanogr.,* **58,** 121–136.

——, X. Xie, P. S. Polito, S.-P. Xie, and H. Hashizume, 2000: Atmospheric manifestation of tropical instability waves observed by QuickSCAT and Tropical Rain Measuring Mission. *Geophys. Res. Lett.,* **27,** 2545–2548.

Ma, J., F. L. Qiao, C. S. Xia, and Y. Z. Yang, 2004: Tidal effects on temperature front in the Yellow Sea. *Chin. J. Oceanol. Limnol.,* **22,** 314–321.

Nitta, T., 1987: Convective activities in the tropical western Pacific and their impact on the Northern Hemisphere summer circulation. *J. Meteor. Soc. Japan,* **65,** 373–390.

Onogi, K., and Coauthors, 2007: The JRA-25 Reanalysis. *J. Meteor. Soc. Japan,* **85,** 369–432.

Pelié, R. J., E. J. Mack, C. W. Rogers, U. Katz, and W. C. Kochmond, 1979: The formation of marine fog and the development of fog-stratus systems along the California coast. *J. Appl. Meteor.,* **18,** 1275–1286.

Ralph, F. M., L. Armi, J. M. Bane, C. Dorman, W. D. Neff, P. J. Neiman, W. Nuss, and P. O. G. Persson, 1998: Observations and analysis of the 10–11 June 1994 coastally trapped disturbance. *Mon. Wea. Rev.,* **126,** 2435–2465.

Slutz, R. J., S. J. Lubker, J. D. Hiscox, S. D. Woodruff, R. L. Jenne, D. H. Joseph, P. M. Steurer, and J. D. Elms, 1985: Comprehensive Ocean–Atmosphere Data Set, release 1. NOAA/Environmental Research Laboratories, Climate Research Program, Boulder, CO, 268 pp.

Su, Y. S., and J. Su, 1996: Low surface temperature belts in the Bohai and Yellow Sea in summer. *Acta Oceanol. Sin.,* **18,** 13–20.

Sverdrup, H., and R. Fleming, 1941: The waters off the coast of southern California. *Bull. Scripps Inst. Oceanogr.,* **4,** 261–378.

——, M. Johnson, and R. Fleming, 1942: *The Oceans: Their Physics, Chemistry, and General Biology*. Prentice-Hall, 1087 pp.

Tao, S. Y., and L. Chen, 1987: A review of recent research on the East Asian summer monsoon in China. *Monsoon Meteorology,* C.-P. Chang and T. N. Krishnamurti, Eds., Oxford University Press, 60–92.

Taylor, G., 1915: Eddy motion in the atmosphere. *Philos. Trans. Roy. Soc. London,* **215A,** 1–26.

——, 1917: The formation of fog and mist. *Quart. J. Roy. Meteor. Soc.,* **43,** 241–268.

Thompson, W. T., T. Haack, J. D. Doyle, and S. D. Burk, 1997: A nonhydrostatic mesoscale simulation of the 10–11 June 1994 coastally trapped wind reversal. *Mon. Wea. Rev.,* **125,** 3211–3230.

——, S. D. Burk, and J. Lewis, 2005: Fog and low clouds in a coastally trapped disturbance. *J. Geophys. Res.,* **110,** D18213, doi:10.1029/2004JD005522.

Tokinaga, H., Y. Tanimoto, S.-P. Xie, T. Sampe, H. Tomita, and H. Ichikawa, 2009: Ocean frontal effects on the vertical development of clouds over the northwest Pacific: In situ and satellite observations. *J. Climate,* **22,** 4241–4260.

Ueda, H., T. Yasunari, and R. Kawamura, 1995: Abrupt seasonal change of large-scale convective activity over the western Pacific in the northern summer. *J. Meteor. Soc. Japan,* **73,** 795–809.

——, M. Ohba, and S.-P. Xie, 2009: Important factors for the development of the Asian–northwest Pacific summer monsoon. *J. Climate,* **22,** 649–669.

Wang, B., and LinHo, 2002: Rainy season of the Asian–Pacific summer monsoon. *J. Climate,* **15,** 386–398.

Wang, B. H., 1983: *Sea Fog* (in Chinese). Ocean Press, 352 pp.

Worley, S. J., S. D. Woodruff, R. W. Reynolds, S. J. Lubker, and N. Lott, 2005: ICOADS release 2.1 data and products. *Int. J. Climatol.,* **25,** 823–842, doi:10.1002/joc.1166.

Xie, P., and P. A. Arkin, 1997: Global precipitation: A 17-year monthly analysis based on gauge observation, satellite estimates and numerical model outputs. *Bull. Amer. Meteor. Soc.,* **78,** 2539–2558.

Xie, S.-P., and N. Saiki, 1999: Abrupt onset and slow seasonal evolution of summer monsoon in an idealized GCM simulation. *J. Meteor. Soc. Japan,* **77,** 949–968.

——, K. Hu, J. Hafner, H. Tokinaga, Y. Du, G. Huang, and T. Sampe, 2009: Indian Ocean capacitor effect on Indo–western Pacific climate during the summer following El Niño. *J. Climate,* **22,** 730–747.

Zhang, H. Y., F. X. Zhou, and X. H. Zang, 2005: Interannual change of sea fog over the Yellow Sea in spring (in Chinese). *Oceanol. Limnol. Sin.,* **36,** 36–42.

Zhang, S. P., and B. Wang, 2008: Global summer monsoon rainy seasons. *Int. J. Climatol.,* **28,** 1563–1578, doi:10.1002/joc.1659.

——, and Z. P. Ren, 2009: The influence of thermal effects of underlaying surface on the spring sea fog over the Yellow Sea—Observations and numerical simulation (in Chinese). *Acta Meteor. Sin.,* in press.

——, ——, J. W. Liu, Y. Q. Yang, and X. G. Wang, 2008: Variations in the lower level of the PBL associated with the Yellow Sea fog—New observation by L-band radar. *J. Ocean Univ. China,* **7,** 353–361, doi:10.1007/s11802-008-0353-1.